Extending the EOS Long-Term $PM_{2.5}$ Data Records Since 2013 in China: Application to the VIIRS Deep Blue Aerosol Products

Jing Wei, *Graduate Student Member, IEEE*, Zhanqing Li, Lin Sun, Wenhao Xue, Zongwei Ma, Lei Liu, Tianyi Fan, and Maureen Cribb

***Abstract*— $PM_{2.5}$ is hazardous to human health, and high-quality data are thus needed on a routine basis. An attempt is made here to improve the accuracy of near-surface $PM_{2.5}$ estimates using the newly released aerosol product derived from the Visible Infrared Imaging Radiometer Suite (VIIRS) satellite with the Deep Blue retrieval algorithm. A high-quality $PM_{2.5}$ data set is generated at a spatial resolution of 6 km from 2013 to 2018 by applying the space-time extremely randomized trees (STET) model, which also aims to extend the Earth Observing System (EOS) long-term $PM_{2.5}$ data records in China. The $PM_{2.5}$ estimates are highly consistent with ground-based measurements, with an out-of-sample cross-validation coefficient of determination (CV-R^2) of 0.88, a root-mean-square error (RMSE) of 16.52 $\mu g/m^3$, and a mean absolute error of 10 $\mu g/m^3$ at the national scale. Spatiotemporal $PM_{2.5}$ variations at monthly scales are also well captured (e.g., $R^2 = 0.91$–0.94, RMSE = 5.8–11.6 $\mu g/m^3$). $PM_{2.5}$ varied greatly at regional and seasonal scales across China. Benefiting from emission reduction and air pollution controls, $PM_{2.5}$ pollution has reduced dramatically in China with an average of -5.6 $\mu g/m^3/yr^{-1}$ during 2013–2018. Significant regional reductions are also seen, in particular, in the Beijing–Tianjin–Hebei region (-6.6 $\mu g/m^3/yr^{-1}$, $p < 0.001$), and the Deltas of Yangtze River (-6.3 $\mu g/m^3/yr^{-1}$, $p < 0.001$) and Pearl River Delta (-4.5 $\mu g/m^3/yr^{-1}$, $p < 0.001$). Our study improved the accuracy of near-surface $PM_{2.5}$ estimates in terms of their spatiotemporal variations at a relatively long-term record, which is important for future air pollution and health studies in China.**

***Index Terms*— Aerosol optical depth (AOD), China, deep blue (DB), $PM_{2.5}$, Visible Infrared Imaging Radiometer Suite (VIIRS).**

Manuscript received September 5, 2020; revised October 19, 2020 and November 23, 2020; accepted January 1, 2021. This work was supported in part by the National Key Research and Development Program of China under Grant 2017YFC1501702, in part by the National Natural Science Foundation of China under Grant 42030606 and Grant 41705125, and in part by the Shanghai Tongji Gao Tingyao Environmental Science and Technology Development Foundation. *(Corresponding authors: Jing Wei; Zhanqing Li.)*

Jing Wei is with the State Key Laboratory of Remote Sensing Science, College of Global Change and Earth System Science, Beijing Normal University, Beijing 100875, China, and also with the Earth System Science Interdisciplinary Center, Department of Atmospheric and Oceanic Science, University of Maryland, College Park, MD 20740 USA (e-mail: weijing_rs@163.com).

Zhanqing Li and Maureen Cribb are with the Earth System Science Interdisciplinary Center, Department of Atmospheric and Oceanic Science, University of Maryland, College Park, MD 20740 USA (e-mail: zli@atmos.umd.edu; mcribb@umd.edu).

Lin Sun is with the College of Geodesy and Geomatics, Shandong University of Science and Technology, Qingdao 266590, China (e-mail: sunlin6@126.com).

Wenhao Xue and Tianyi Fan are with the College of Global Change and Earth System Science, Beijing Normal University, Beijing 100875, China (e-mail: xuewh@mail.bnu.edu.cn; fantianyi@bnu.edu.cn).

Zongwei Ma is with the State Key Laboratory of Pollution Control and Resource Reuse, School of the Environment, Nanjing University, Nanjing 210023, China (e-mail: zma@nju.edu.cn).

Lei Liu is with the College of Earth and Environmental Sciences, Lanzhou University, Lanzhou 730000, China (e-mail: liuleigeo@lzu.edu.cn).

Color versions of one or more figures in this article are available at https://doi.org/10.1109/TGRS.2021.3050999.

Digital Object Identifier 10.1109/TGRS.2021.3050999

I. Introduction

AIR pollution has a great influence on atmospheric visibility, human health, climate, and the ecosystem and has thus been a major global problem [1]–[5]. Atmospheric $PM_{2.5}$ is of particular concern to human health. The World Health Organization has reported that 90% of the world's population live in dangerous environments shrouded in $PM_{2.5}$, which is highly associated with cardiovascular, cerebrovascular, and respiratory diseases [6]–[10], increases in premature mortality [11]–[14], the harming of fetuses during pregnancy [15], [16], and causing brain problems and memory decline [17]. In particular, China has experienced increasing levels of $PM_{2.5}$ pollution in recent decades caused by rapid urbanization and industrialization [18], [19]. Therefore, high-quality $PM_{2.5}$ data are urgently needed, a key for understanding the formation and control of air pollution and their effects on human health.

While there have existed some ground-based PM observation networks in China, they are generally of short durations and highly inhomogeneous. In contrast, remote sensing technology allows for deriving ground-level $PM_{2.5}$ distributions on a global scale at uniform resolutions. Given its long-term data records since 2000, short revisiting period, and mature aerosol retrieval algorithms, MODIS aerosol products, i.e., dark target (DT) and deep blue (DB) products at 3–10-km spatial resolution, have been widely used in $PM_{2.5}$ estimations [20]–[23]. Later, Visible Infrared Imaging Radiometer Suite (VIIRS) was launched on October 28, 2011, and NOAA has released a series of operational VIIRS Environmental Data Records (EDRs), including daily aerosol products (VAOOO) at a 6 km spatial resolution, generated using a DT-like algorithm [24]. These data have been available to the public since May 2012.

Wu *et al.* [25] proposed a spatiotemporal statistical model to derive $PM_{2.5}$ concentrations from VIIRS VAOOO aerosol optical depth (AOD) products in the Beijing–Tianjin–Hebei (BTH) region of China. The $PM_{2.5}$ estimates are well related to

ground measurements with an out-of-sample cross-validation (CV)-R^2 of 0.72. Pang *et al.* [26] forecast $PM_{2.5}$ concentrations by assimilating VIIRS VAOOO and Geostationary Ocean Color Imager (GOCI) AOD products using a 3-D variational assimilation system in the BTH and Pearl River Delta (PRD) regions with out-of-sample CV-R^2 values of 0.62 and 0.51, respectively. Yao *et al.* [27] used a time-fixed-effects regression model and compared the model performance in daily $PM_{2.5}$ estimates using MODIS DT and VIIRS VAOOO AOD products in the BTH region with varying out-of-sample CV-R^2 values ranging from 0.55 to 0.72. Later, they proposed a spatially structured adaptive two-stage model to obtain the $PM_{2.5}$ concentrations in China with an out-of-sample CV-R^2 of 0.60 [28].

However, these traditional statistical regression methods are difficult to construct robust $PM_{2.5}$-AOD relationships due to the complex sources affecting $PM_{2.5}$ and weak data-mining abilities. In addition, aerosol remote sensing still faced great challenges over bright and heterogeneous surfaces, showing large estimation uncertainties and numerous missing values [29], [30]. Therefore, the data quality of $PM_{2.5}$ estimates derived from the VIIRS VAOOO AOD products is much poor (i.e., CV-R^2 = 0.51–0.72). In particular, there are few studies on $PM_{2.5}$ estimates using the VIIRS aerosol products. As an extension and improvement on the AVHRR and the MODIS, VIIRS will have great application potential for future atmospheric environment monitoring. In addition, the widely used MODIS satellites have been in service for more than 20 years, although still in operation, well exceeding its design life. On February 6, 2018, NASA released the VIIRS AERDB products at the same 6-km resolution by applying the MODIS DB algorithm [31] to extend the Earth Observing System (EOS) long-term aerosol data records [32]. Different from the VAOOO DT algorithm, the DB algorithm allows aerosol retrieval from the darkest to the brightest surfaces, resulting in an AOD data set with a more complete spatial coverage [33].

Bearing the above problems in mind, the main objective of this study is to improve the accuracy of ground-level $PM_{2.5}$ estimates and to extend the EOS long-term $PM_{2.5}$ data records in China from the VIIRS satellite. For this purpose, based on our previous study [34], the space-time tree-based machine learning (ML) models are involved but with several improvements, including the variable update according to the physical mechanisms and improved determination of spatiotemporal information. Then, the high-quality $PM_{2.5}$ data set at a 6-km resolution from 2013 to 2018 in China is obtained from the newly released VIIRS DB AOD product. The spatiotemporal variations of $PM_{2.5}$ pollution in China were also investigated. In addition, an in-depth analysis of the model performance and sensitivity is also performed.

II. Data Sources

A. $PM_{2.5}$ in Situ Data

In this study, hourly $PM_{2.5}$ measurements from 2013 to 2018 are collected here, and the number of monitoring stations has been increasing in this period: 835, 940, 1480, 1484, 1568, and 1583 for 2013–2018, respectively, evenly distributed across Eastern China. Most land surface types exist, including three typical urban agglomerations located in eastern China, i.e., the BTH region, the Yangtze River Delta (YRD) region, and the PRD region, where human activities are intensive (Fig. 1). In our study, similar to previous studies [20]–[23], [28], all hourly measurements are averaged to obtain the daily $PM_{2.5}$ concentrations at each monitoring station in a day of one year. In addition, if there are two or more $PM_{2.5}$ monitoring stations in a pixel, all available $PM_{2.5}$ measurements are averaged.

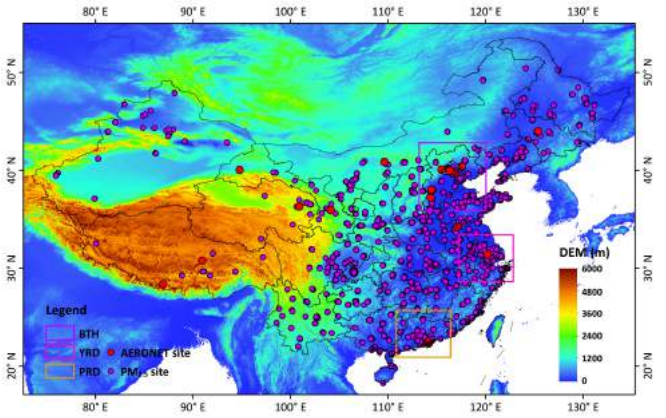

Fig. 1. Spatial distributions of surface $PM_{2.5}$ (pink dots) and AERONET (red dots) monitoring stations in China.

B. VIIRS DB AOD Product

In this study, the VIIRS AERDB DB Level 2 AOD product (Version 1) at a spatial resolution of 6 km from 2013 to 2018, covering entire China, is employed. Different from the VIIRS DT product, it is generated based on the DB algorithm over land [32] and the Satellite Ocean Aerosol Retrieval (SOAR) algorithm over the ocean [35]. The main algorithm difference is the determination of the surface reflectance, which allows for aerosol retrievals regardless of surface brightness. It works in a similar way to the MODIS second-generation DB algorithm [31] but with main updates in the radiative transfer model, smoke detection, and aerosol type assumption [32]. Here, only AERDB DB AOD retrievals (550 nm) passing the quality assurance are used as the main independent variable for retrieving the ground-level $PM_{2.5}$ concentrations.

C. Auxiliary Influence Variables

There are numerous (natural and human) factors affecting the conversion from satellite AOD to near-surface $PM_{2.5}$ concentrations. Meteorological conditions show obvious influences on air pollution, in which boundary layer height (BLH) is selected to reflect the vertical distributions of aerosol particles [36]–[39]. Relative humidity (RH) and temperature (TEM) are two main factors affecting the hygroscopic growth of aerosol particles [39]–[41]. In addition, precipitation (PRE), evaporation (ET), and surface pressure (SP) can promote the production or removal of $PM_{2.5}$ [34], [42], [43]. Wind speed (WS) and wind direction (WD) can affect the transmission of $PM_{2.5}$ from different directions [38], [44]. Meanwhile, land-use cover (LUC),

Normalized Difference Vegetation Index (NDVI), and Digital Elevation Model (DEM) are selected to reflect the surface conditions. Because the land surface types vary greatly across China, the terrain variations can affect the diffusion of air pollutants [44], [45]. Anthropogenic aerosols are another main source of $PM_{2.5}$, in which the population distribution (POP) and nighttime light (NTL) are selected to represent the density of human activities. Furthermore, pollutant emissions (i.e., PM, NH_3, NO_x, and SO_2) originating from industry, transportation, power, and residences with small uncertainties obtained from the MEIC inventory are employed to characterize the $PM_{2.5}$ direct emissions or generations via chemical reactions [46], [47]. Therefore, a total of 18 auxiliary independent variables are selected in this study. All auxiliary data are first resampled to a uniform 6 km resolution to be consistent with the VIIRS DB AOD product.

III. Methodology

A. Model Introduction and Adjustment

In this study, four popular tree-based ML methods, including the decision tree (DCT), gradient tree boosting (GDBT), random forest (RF), and extremely randomized trees (ERT), are considered. The decision tree is a binary or nonbinary tree structure, which is a simple and easy-to-use nonparametric regressor or classifier that does not need any prior hypothesis about the data. There are three main kinds of decision-tree-building algorithms, including the ID3, C4.5, and CART. The GDBT model is based on the boosting sampling and the CART algorithm, which has a good mixed-data processing ability, strong prediction ability, and robustness to outliers in outputs. However, all learners are ordered, making parallel computing difficult [48]. The RF model is based on the bagging sampling and ID3 and C4.5 algorithms, and all learners are totally independent, allowing for parallel computing. It can efficiently process a large number of input data and generate an unbiased estimate and is not easy to be overfitted [49]. The ERT model works like the RF model, but all samples are used in the data sampling in extra-trees building, and besides the attribute, splitting is completely random [50]. For the tree-based ensemble learning methods, there are five main steps taken during the model training.

1) *Sample Random Selection:* A new sample subset (n) is randomly selected from a given training sample set (N) using different data sampling methods, such as bagging or boosting.
2) *Feature Random Selection:* m attributes are randomly selected from a total of M features meeting the condition $m \ll M$. The best feature is then determined as the split attribute of the node according to a strategy, such as information gain (rate) or the Gini index.
3) *Model Training:* For tree-based ML models, two main hyper-parameters, i.e., the maximum number of weak learners and the maximum depth of the decision tree, need to be set, and the optimal combination is determined by the iterative method.
4) *Decision-Tree Construction:* Based on the above-selected samples and features, a decision tree can be established by selecting an appropriate method such as ID3, C4.5, or CART.
5) *Final Result Output:* Repeat the above three steps h times to generate H decision trees. Last, for the regression problem, the final result is calculated based on the mean value of the outputs of all decision trees. Detailed information can be found in their algorithm documents [48]–[50].

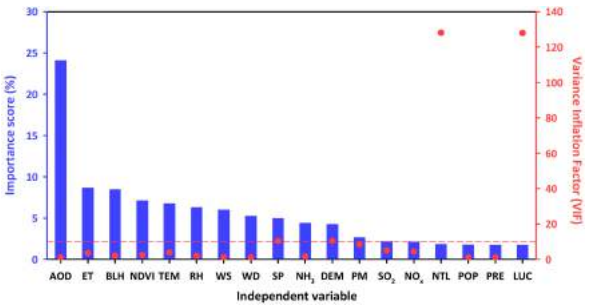

Fig. 2. VIFs (red dots) and sorted importance scores (blue bars) of each predictor in $PM_{2.5}$ estimates in China.

However, air pollution is spatiotemporally heterogeneous, i.e., $PM_{2.5}$ concentrations change dramatically over space and time, an issue that most previous studies have always neglected. Therefore, spatiotemporal information is introduced into these tree-based ML models to improve the $PM_{2.5}$–AOD relationships in China. Different from our previous study [34], the spatial term (*Space*) is further optimized and represented by the latitude and longitude of a point in space and its great-circle distances to four corners, i.e., top left, top right, bottom right, and bottom left, as well as the center of the defined rectangle study region using the Haversine approach [34]. They can more accurately describe the spatial autocorrelation and difference of a point in space [51]. The temporal term (*Time*) is simplified as a day of the year to identify each row of data records on different days in a year since air pollution is different every day. Thus, these corresponding models by involving the spatiotemporal information, i.e., STDT, STGT, STRF, and space-time extremely randomized trees (STETs), are defined.

Meanwhile, five traditional statistical regression models, i.e., the multiple linear regression (MLR) model, the linear mixed-effect (LME) model, the geographically weighted regression (GWR) model, the geographically and temporally weighted regression (GTWR) model, and the two-stage model, are also employed for comparison.

Due to a large number of selected variables, there will be inevitable multivariable collinearity problems that most models are susceptible to, especially for traditional statistical regression models. Therefore, the variance inflation factor (VIF) approach is first applied to see which level the predictors are independent of each other [10]. The diagnosis results show that the VIF values between LUC and NTL are extremely high >120, indicating strong collinearities. By contrast, most of the other selected predictors are independent of each other with small VIF values <10 (Fig. 2). Therefore, we prefer to remain the factors with higher temporal resolutions (i.e., NTL) to avoid multicollinearity among the predictors.

In addition, different from other traditional statistical regression and artificial intelligence models, the tree-based ensemble ML approaches provide a new and effective way, i.e., importance score, to quantitatively measure the importance of each input predictor during the model training using the Gini Index [34], [52]. This procedure can minimize the overfitting issue and improve the model efficiency. In this study, the process is done for all tree-based ensemble learning models, and the orders of the sorted importance scores of each predictor in $PM_{2.5}$ estimates in China are the same (Fig. 2). AOD is the most important variable, with an average importance score of 24%. Seven meteorological variables (i.e., ET, BLH, TEM, RH, WS, WD, and SP) and two surface-related variables (i.e., NDVI and DEM) show large influences on $PM_{2.5}$ estimates. In addition, four pollutant emissions (i.e., NH_3, PM, SO_2, NO_x) are also important. By contrast, the remaining four variables (i.e., NTL, POP, PRE, and LUC) are less important, so they are excluded from each model.

Therefore, five traditional statistical regression methods and five original tree-based ML models with the same input variables can be expressed as

$$\mathrm{PM}_{2.5} = f_x[\mathrm{AOD}, \mathrm{BLH}, \mathrm{ET}, \mathrm{RH}, \mathrm{SP}, \mathrm{TEM}, \mathrm{WD}, \mathrm{WS}, \mathrm{NDVI}, \mathrm{DEM}, \mathrm{NH_3}, \mathrm{NO}_x, \mathrm{PM}, \mathrm{SO_2}]. \quad (1)$$

However, five newly defined space-time tree-based ML models with two additional inputs of spatial and temporal information can be expressed as

$$\mathrm{PM}_{2.5\mathrm{st}} = f_{\mathrm{STx}}[\mathrm{AOD}_{\mathrm{st}}, \mathrm{BLH}_{\mathrm{st}}, \mathrm{ET}_{\mathrm{st}}, \mathrm{RH}_{\mathrm{st}}, \mathrm{SP}_{\mathrm{st}}, \mathrm{TEM}_{\mathrm{st}}, \mathrm{WD}_{\mathrm{st}}, \mathrm{WS}_{\mathrm{st}}, \mathrm{NDVI}_{\mathrm{st}}, \mathrm{DEM}_{\mathrm{st}}, \mathrm{NH}_{3\mathrm{st}}, \mathrm{NO}_{\mathrm{xst}}, \mathrm{PM}_{\mathrm{st}}, \mathrm{SO}_{2\mathrm{st}}, \mathrm{Space}, \mathrm{Time}]. \quad (2)$$

B. Evaluation and Analysis Approaches

Here, the widely used out-of-sample tenfold cross-validation (10-CV) method [53] is selected to evaluate the $PM_{2.5}$ estimates. However, our study aims to retrieve $PM_{2.5}$ concentrations in areas where ground monitoring stations are not available. Thus, an additional independent out-of-station 10-CV approach is applied to evaluate the spatial prediction ability of the model [34], [54]. It is performed based on the $PM_{2.5}$ monitoring stations using the 10-CV approach, i.e., the $PM_{2.5}$ monitoring stations are randomly divided into ten groups, then the data samples collected from 9 groups and the remaining 10th group of monitoring stations are used for training and validation, respectively. It is done ten times, in turn, to ensure all the monitoring stations are tested. This method can ensure that the training and testing samples are made up of different spatial points in different locations, where the surface and atmospheric conditions may be different, which would influence the results.

For spatiotemporal analysis, daily $PM_{2.5}$ values are averaged to generate monthly $PM_{2.5}$ maps, and then they are used to synthesize the annual and seasonal $PM_{2.5}$ maps in China. The area-weighting approach is selected to calculate the spatial coverage. $PM_{2.5}$ trends are calculated from deseasonalized monthly $PM_{2.5}$ anomalies, and the significance of the trends is determined using the two-sided test [55].

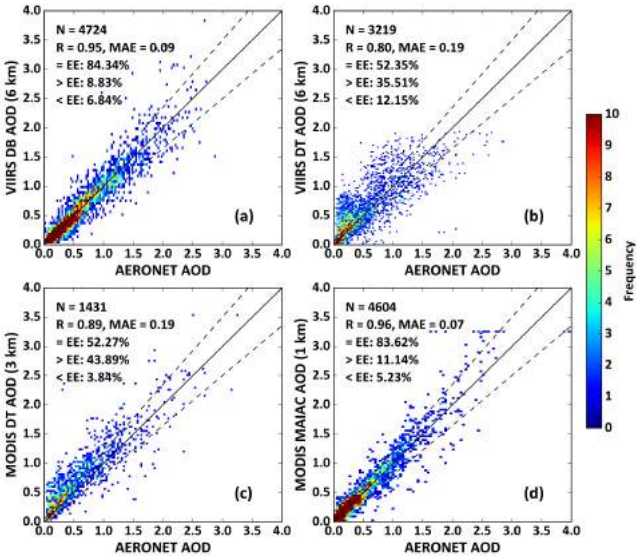

Fig. 3. Validation and comparison of (a) VIIRS DB (6 km), (b) VIIRS DT (6 km), (c) MODIS DT (3 km), and (d) MODIS MAIAC (1 km) AOD products from 2013 to 2018 in China.

IV. Results and Discussion

A. Validation and Comparison of Different AOD Products

We first validate and compare the VIIRS DB (6 km) and DT (6 km), MODIS DT (3 km) and MAIAC (1 km) AOD products against ground-based measurements collected at 22 AERONET sites (containing nine urban and 11 vegetated sites) in China (Fig. 3) using the spatiotemporal matching method [33]. Results show that VIIRS DB retrievals are highly related to AERONET AODs ($R = 0.95$) with a mean absolute error (MAE) of 0.09, and 84.34% of the matchups falling within the commonly used expected error (EE, $\pm$ [0.05% $\pm$ 20%]). By contrast, VIIRS DT and MODIS DT (3 km) retrievals yield much lower accuracy with larger MAEs of 0.19, and only 52% of them falling within the EE, showing significant overestimations. The retrieval errors mainly come from urban areas due to the inaccuracy of surface reflectance estimates. In particular, the sample size has been reduced by 1.5–3.3 times because the DT algorithm cannot work over bright surfaces, showing a large number of missing values [29], [30]. However, the number of data samples of VIIRS DB product ($N = 4724$) is larger than the MODIS MAIAC product ($N = 4604$), in addition, VIIRS DB AODs show a comparable accuracy with MODIS MAIAC AODs but with a higher proportion of the retrievals falling within the EE. These results illustrated that the VIIRS DB product has a slightly wider spatial coverage and a higher accuracy, and thus it is selected here to improve the $PM_{2.5}$ estimations.

B. Model Validation and Comparison

Since there are few studies working on $PM_{2.5}$ estimates using the VIIRS AOD products, five traditional statistical regression models, four original and four space-time tree-based ML methods are selected to test and compare their performance in $PM_{2.5}$ estimates in China using the same input data in 2018 (Table I). Among five statistical regression models,

TABLE I
COMPARISON OF MODEL PERFORMANCES OF DIFFERENT MODELS IN CHINA USING THE SAME INPUT DATA IN 2018

Model	Out-of-sample validation			Out-of-station validation		
	R^2	RMSE	MAE	R^2	RMSE	MAE
MLR	0.38	17.32	19.16	0.37	18.31	20.14
GWR	0.55	16.97	16.12	0.54	17.88	17.32
LME	0.67	16.48	13.43	0.66	17.42	14.56
Two-stage	0.70	16.27	12.82	0.69	17.31	13.70
GTWR	0.77	15.98	10.73	0.76	17.15	11.84
DCT	0.64	21.98	13.55	0.60	23.63	14.51
GBDT	0.67	20.13	12.61	0.64	20.97	13.37
RF	0.81	15.41	9.74	0.78	16.28	10.43
ERT	0.82	14.59	9.23	0.81	15.28	9.82
STDT	0.76	17.50	11.97	0.75	17.79	12.33
STGT	0.78	16.25	10.89	0.77	16.84	11.39
STRF	0.87	12.32	7.59	0.86	12.76	8.04
STET	0.89	11.48	7.12	0.88	12.14	7.72

the MLR model works the worst with the lowest CV-R^2 values and largest root-mean-square error (RMSE) and MAE values, which significantly underestimated the $PM_{2.5}$ concentrations. However, the performance of the GWR model is somewhat better with higher CV-R^2 values and smaller RMSE and MAE values, mainly because the spatial heterogeneity of $PM_{2.5}$ is considered. The LME model performs even better with overall better evaluation indicators because the mixed-effects among different influence factors are considered. The two-stage model performs much better with improved validation results because it combines the advantages of the GWR and LME models. The GTWR model performs the best with the highest CV-R^2 values and smallest uncertainties, mainly due to the involvement of both spatial and temporal information.

Regarding tree-based ML methods, the original DCT and GDBT models perform poorly with overall low CV-R^2 values and large estimation uncertainties. However, the RF model performs much better than all the above-mentioned models with higher CV-R^2 values and smaller RMSE and MAE values because of its more effective and random data sampling and feature selection [49]. In addition, the ET model is overall better than the RF model due to its stronger randomness in feature selection and node splitting during the decision-tree building [50]. However, when considering the spatiotemporal characteristics of $PM_{2.5}$ concentrations, the performance of all tree-based ML approaches has significantly improved with all better evaluation indicators. In general, the STET model shows the best performance in estimating and predicting $PM_{2.5}$ concentrations with the highest CV-R^2 values and the smallest uncertainties among all the selected models.

C. Validation of $PM_{2.5}$ Estimates From 2013 to 2018

In this study, the STET model is developed based on all the data samples for each year from 2013 to 2018 separately. Fig. 4 shows the out-of-sample and out-of-station CV results of daily $PM_{2.5}$ estimates against ground measurements for each year from 2013 to 2018 in China. It should be noted that there are some numerical differences in evaluation metrics, possibly due to different ranges of $PM_{2.5}$ loadings among different years. The sample-based CV results show that the $PM_{2.5}$ estimates are highly correlated with the surface observations with CV-R^2 values ranging from 0.86 to 0.89 among different years across China. Most of the data samples are concentrated along the regression lines of strong slopes 0.83–0.87 and small y-intercepts of 6.6–12.5 $\mu g/m^3$, especially in the range of 0–200 $\mu g/m^3$, which has the highest distribution density. The estimation uncertainties are generally small, with average RMSEs and MAEs of 11.4–22.6 $\mu g/m^3$ and 7.1–14 $\mu g/m^3$, respectively. In general, the overall accuracy of the STET model reaches up to 0.88 with an average RMSE of 16.52 $\mu g/m^3$ and an MAE of 10 $\mu g/m^3$ during 2013–2018 in China, respectively.

For station-based CV results, the $PM_{2.5}$ predictors are well consistent with ground measurements with varying CV-R^2 from 0.83 to 0.88, showing overall low prediction uncertainties with RMSE and MAE values of 12.1–23.8 and 7.7–15 $\mu g/m^3$ over the years across China. Similarly, the regression lines also have strong slopes of 0.82–0.86 and small y-intercepts of 7.1–13.3 $\mu g/m^3$. In general, the STET model has a strong spatial prediction ability with a CV-R^2 equal to 0.87, and the average RMSE and MAE are 17.53 and 10.86 $\mu g/m^3$, respectively. Furthermore, compared with the out-of-sample CV results, the out-of-station CV results decrease smaller in most evaluation indexes, further demonstrating the robustness of the model.

Fig. 5 shows the regional CV results over Eastern China and three typical urban agglomerations during 2013–2018. The model is highly accurate with sample- and station-based CV-R^2 values of 0.89 and 0.88, respectively, showing overall small uncertainties (i.e., RMSE = 16.39 and 17.12 $\mu g/m^3$) over eastern China. The model yields the highest CV-R^2 ($\sim$0.89–0.9) but the largest RMSE ($>$19 $\mu g/m^3$) and MAE ($>$11 $\mu g/m^3$) values in the BTH region due to severe air pollution with a large number of data samples $>$300 $\mu g/m^3$. Followed by the YRD region (e.g., CV-R^2 = 0.88–0.89, RMSE = 13–14 $\mu g/m^3$). By contrast, the model yields the lowest CV-R^2 ($<$0.86) and the smallest RMSE ($<$12 $\mu g/m^3$) and MAE ($<$8 $\mu g/m^3$) values in the PRD region where air pollution is much slighter with most days $<$150 $\mu g/m^3$. Besides the low air pollution, more frequent clouds (e.g., reduce the number of the data samples) and wetter climate conditions (e.g., abundant precipitation and high RH) further increase the difficulties of $PM_{2.5}$ estimates in China [34], [38].

Fig. 6 shows the individual-scale CV results from 2013 to 2018 across China. For sample-based CV results, our daily $PM_{2.5}$ estimates are highly consistent with ground measurements with small uncertainties at most sites in China, showing overall small uncertainties, especially the North China Plain (e.g., CV-R^2 $>$ 0.9). By contrast, several monitoring stations located in Northwest China show overall poor accuracy with low CV-R^2 and large RMSE values because of the sparse site distributions and high $PM_{2.5}$-polluted conditions. In general, approximately 72% and 83% of the monitoring stations have CV-R^2 $>$ 0.8 and RMSEs $<$18 $\mu g/m^3$, respectively. Furthermore, the station-based CV results show similar spatial patterns with the sample-based CV results, but the CV-R^2 values are slightly smaller, yet the RMSE values are larger overall at most stations across China. In general, except for

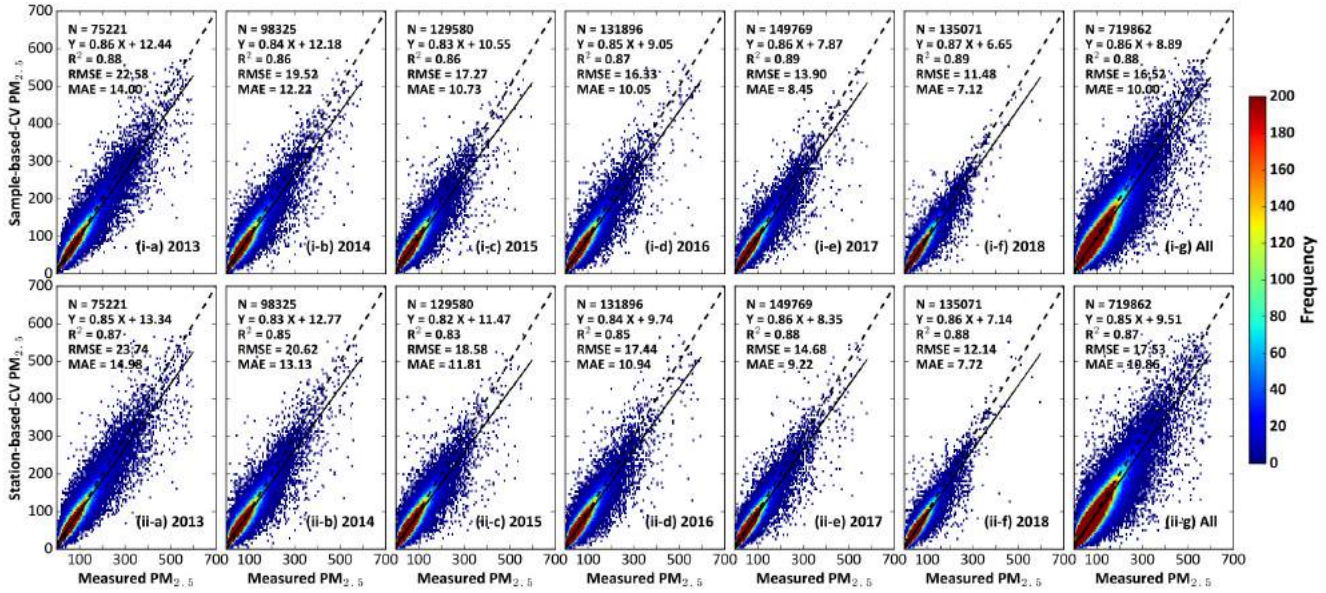

Fig. 4. Density scatterplots of (a–f) out-of-sample and (g–l) out-of-station CV results of daily $PM_{2.5}$ estimates from 2013 to 2018 in China.

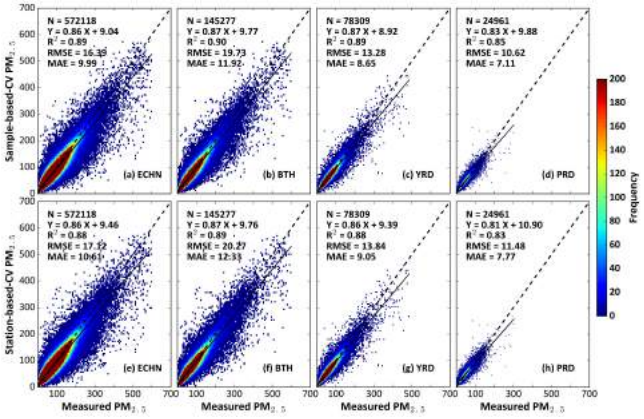

Fig. 5. Density scatterplots of regional (a)–(d) out-of-sample and (e)–(h) out-of-station CV results of daily $PM_{2.5}$ estimates during 2013–2018.

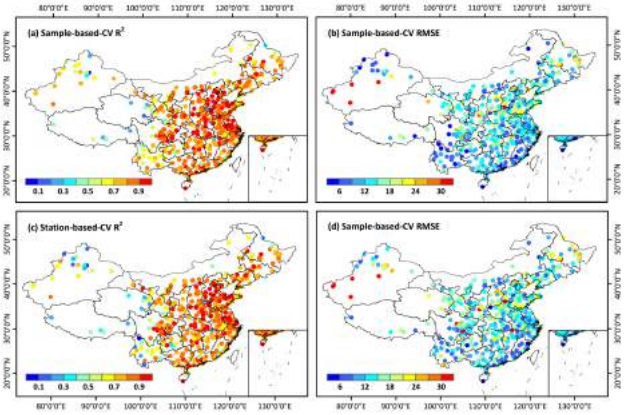

Fig. 6. Spatial distributions of (a) and (b) out-of-sample and (c) and (d) out-of-station CV results of daily $PM_{2.5}$ estimates from 2013 to 2018 at each monitoring station in China.

several individual stations, our model shows strong prediction ability at most stations, and approximately 69% and 77% of the stations have high CV-R^2 (>0.8) and small RMSE (<18 $\mu g/m^3$) values. These results illustrate that the STET model performs well in estimating and predicting $PM_{2.5}$ concentrations at different locations in China, especially in areas without ground monitoring stations.

D. Discussion

1) Sensitivity Analysis and Model Comparison: First of all, we analyzed the sensitivity of the selected predictors to $PM_{2.5}$ estimates using the STET model by adding varying noises (covering from space to time) from 1% to 20% to each variable in the training data from 2018 in China (Fig. 7). In general, the absolute mean relative errors of $PM_{2.5}$ estimates become larger with increasing uncertainties in each input variable; however, the sensitivity of different variables to $PM_{2.5}$ estimates varies greatly and show no-linear relationships. AOD is the most sensitive predictor to $PM_{2.5}$ estimates, and a 1% retrieval errors can lead to about 0.13% errors in $PM_{2.5}$ estimates. Followed by NDVI and all meteorological factors that have decreasing slopes ranging from 0.03 to 0.07. By contrast, our model is less sensitive to DEM and four pollutant emissions with much smaller slopes <0.02. These results illustrate that our model is robust and noise resistant, benefiting from the advantages of tree-based ensemble learning [48]–[50]. In addition, our results also confirmed the complexity and uncertainty of various factors affecting $PM_{2.5}$, among which AOD, underlying surfaces, and meteorological conditions are particularly useful for $PM_{2.5}$ inversion and need to be determined accurately.

Furthermore, we compare the model performance with different input variables in $PM_{2.5}$ estimates in China using the data in 2018. First, when the predictors with lower important scores are retained, the accuracy and prediction ability of the model are overall decreased. The sources for the biases mainly are that most of these variables are at lower temporal resolutions (e.g., annual), or their values change little in a year, which provides less valuable information but introduces additional noises. These results illustrate that it is necessary

TABLE II
MODEL PERFORMANCE STATISTICS FROM THIS STUDY AND PREVIOUS STUDIES FOCUSED ON CHINA

Model	Model validation (out-of-sample)			Study period	Study region	AOD product	Spatial resolution
	R^2	RMSE (μg/m^3)	MAE (μg/m^3)				
Two-stage	0.72	19.29	12.27		BTH	VIIRS DT	6 km
Time-fixed effects	0.72	22.07	15.23		BTH	VIIRS DT	6 km
Data assimilation	0.62	-	-		BTH	VIIRS DT	6 km
	0.51				PRD	VIIRS DT	6 km
Two-stage	0.60	21.76	14.41	2014	China	VIIRS DT	6 km
Two-stage	0.77	17.10	11.51	2017	China	MODIS DT	10 km
GWR	0.79	20.85	-	2014	China	MODIS DT	10 km
	0.85	24.86	-		China	MISR	17.6 km
TSAM	0.80	22.75	15.99	2013-2014	China	MODIS DT	10 km
Gaussian	0.81	21.87	-	2013	China	MODIS DT and DB	10 km
ML	0.61	27.8-	-	2013-2016	China		
GRNN	0.67	20.93	13.90	2013-2014	China	MODIS DT	3 km
GWR	0.79	18.60	-	2014	China	MODIS DT	3 km
GTWR	0.80	18.00	12.03	2015	China	MODIS DT	3 km
XGBoost	0.86	14.98	-	2014-2015	China	MODIS DT	3 km
STRF	0.85	15.57	9.77	2016	China	MODIS MAIAC	1 km
STET	0.89	10.35	6.71	2018	China	MODIS MAIAC	1 km

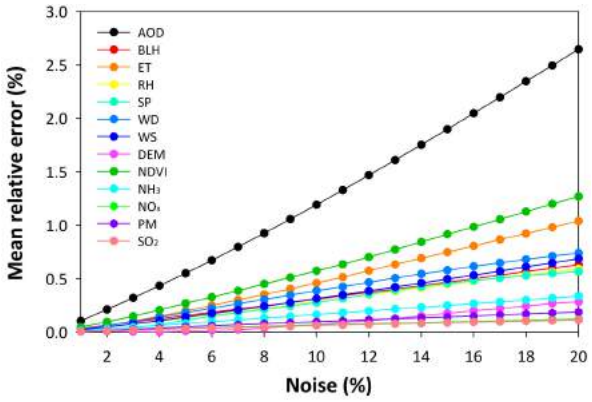

Fig. 7. Variation of the mean relative error (%) in $PM_{2.5}$ estimates with increasing noises for each input predictor using the STET model in China.

to perform the appropriate feature screening because this procedure can improve not only the overall accuracy but also the operation efficiency.

Then, we compared the model performance by remaining the emissions or AOD due to their same positive correlations with surface $PM_{2.5}$ concentrations. Results show that the model performance without AOD decreased obviously with much lower CV-R^2 values and larger RMSEs. By contrast, the model performance without pollutant emissions decreases slightly with relatively small differences in CV-R^2 and RMSE values <0.02 and <1, respectively. The main reason is that AOD has much higher spatial (i.e., $0.06^\circ \times 0.06^\circ$) and temporal (e.g., daily) resolutions than the emissions (i.e., $0.25^\circ \times 0.25^\circ$, monthly), which can provide more detailed spatiotemporal information. In addition, the correlations between $PM_{2.5}$ observations and AOD are significantly higher (i.e., $R = 0.49$, $p < 0.01$) than that between $PM_{2.5}$ and emissions (i.e., $R < 0.12$, $p < 0.05$), further explaining this.

2) Comparison With Related $PM_{2.5}$ Studies: In this section, we first compare our results with previous related $PM_{2.5}$ studies using the same VIIRS AOD products (Table II). Results show that our STET model is superior to the time-fixed effects regression model [25] and the spatiotemporal statistical model combining the time-fixed effects regression and GWR models [27] in the BTH region. It performs much better than the 3-D variational data assimilation model in the BTH and YRD regions [26]. Furthermore, it outperforms the spatially structured adaptive two-stage model at the national scale [28]. The main reason is that our algorithm yields a much stronger data mining ability than traditional methods. In addition, we also performed a model comparison with VAOOO AOD products using the same approach with the data in 2018. The model performance has slightly decreased with decreasing CV-R^2 values and increasing RMSE values. Therefore, systematic bias may not have a significant impact on ML approaches. Nevertheless, the data quality of AOD product may be another potential reason because VIIRS DT AOD product is less accurate with a narrower spatial coverage than VIIRS DB AOD product in China. Therefore, the resulting aerosol estimation uncertainties and the reduction of data samples may influence the results to a certain extent.

Then, we also compare our results with previous related studies focusing on China that are based on different satellites. Our $PM_{2.5}$ estimates are more accurate at a higher spatial resolution (6 km) than those retrieved from either MODIS or MISR AOD products at coarser spatial resolutions of 10–17.6 km using the two-stage model [56], the GWR model [57], the timely structure adaptive modeling (TSAM) [21], and the Gaussian model [45] across China, respectively. In addition, although lower spatial resolution, our data yield higher accuracy and wider spatial coverage than those derived from the defined ML model [22], the generalized regression neural network (GRNN) model [59], the GWR model [60], the GTWR model [23], and the extreme gradient boosting (XGBoost) model [61], respectively, based on MODIS 3-km DT AOD products, which have a large number of missing values [62], [63]. Last, our model outperforms the STRF model [10] and shows a comparable accuracy with an equal CV-R^2 to the STET model [34] developed for MODIS MAIAC 1-km AOD products in our previous studies. These results illustrate that

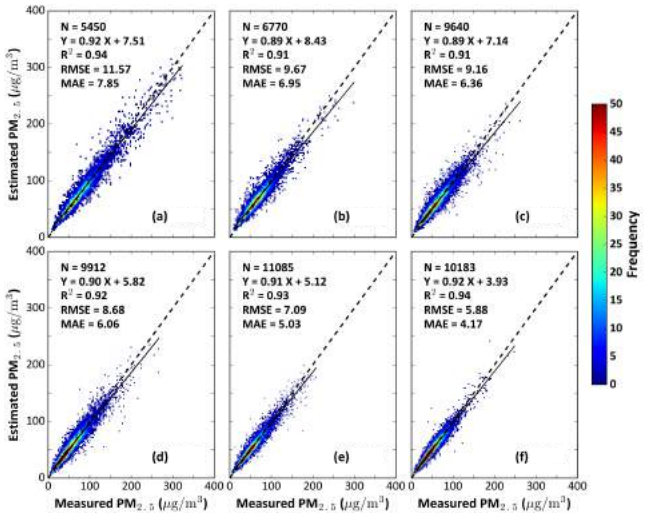

Fig. 8. Validation of monthly mean $PM_{2.5}$ estimates from all monitoring stations for each year from 2013 to 2018 across China (a) 2013, (b) 2014, (c) 2015, (d) 2016, (e) 2017, and (f) 2018.

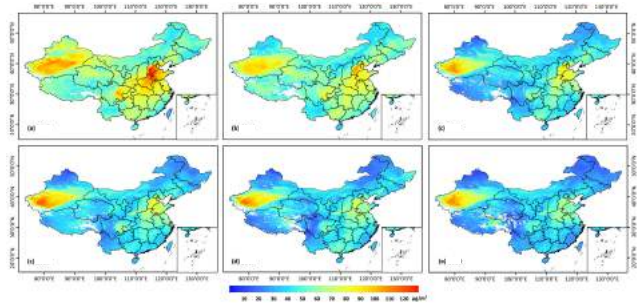

Fig. 9. VIIRS-DB-derived annual mean $PM_{2.5}$ maps (6 km) for each year from 2013 to 2018 in China (a) 2013, (b) 2014, (c) 2015, (d) 2016, (e) 2017, and (f) 2018.

our model is superior to most models developed in previous studies for different satellites; in addition, it has a strong universality and works well on different satellites. Moreover, we will extend our model to the forthcoming VIIRS MAIAC 750-m AOD product to further improve the spatial resolution of the $PM_{2.5}$ data set in China in a future study.

V. Spatiotemporal Variations Across China

A. Spatial Coverage and Distribution

The daily $PM_{2.5}$ maps are generated using the STET model in China, then the monthly, seasonal, and annual maps are synthesized using our previous approach [34]. First, monthly mean $PM_{2.5}$ concentrations are calculated and validated against surface observations at each monitoring station for each year (Fig. 8). The monthly $PM_{2.5}$ matchups are highly consistent (i.e., R^2 = 0.91–0.94, slope = 0.83–0.89), showing small estimation uncertainties (i.e., RMSE = 5.8–11.6 μg/m^3 and MAE = 4.1–7.9 μg/m^3) among different years during the study period in China. These results suggest that our $PM_{2.5}$ data set can more accurately describe the spatiotemporal variations in $PM_{2.5}$ pollution across China.

Fig. 9 illustrates annual $PM_{2.5}$ maps (6 km) covering mainland China derived from the VIIRS DB aerosol product using the STET model from 2013 to 2018. Except for Qinghai province spread across the Tibetan Plateau where the DB

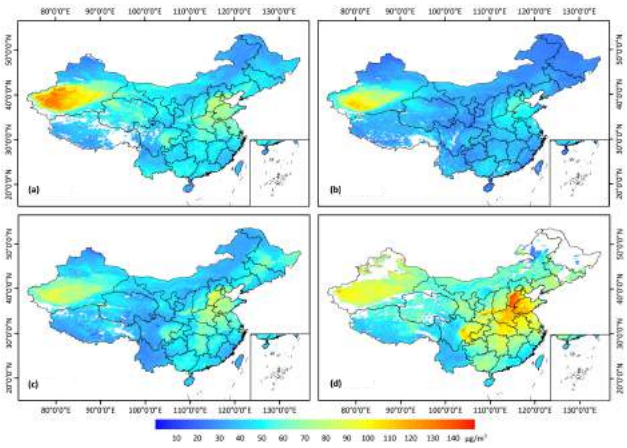

Fig. 10. VIIRS-DB-derived seasonal mean $PM_{2.5}$ maps (6 km) during 2013–2018 in China (a) Spring, (b) Summer, (c) Autumn, and (d) Winter.

algorithm does not work, our model can generate complete and spatially continuous annual $PM_{2.5}$ maps, with the spatial coverage ranging from 95% to 98% (average = 96%) in China. In addition, $PM_{2.5}$ pollution varies from year to year in China with an annual mean value of 67.0 ± 17.6, 58.4 ± 13.4, 45.2 ± 16.4, 44.2 ± 17.7, 41.7 ± 16.8, and 38.2 ± 17.2 μg/m^3 in each consecutive year from 2013 to 2018, respectively.

In terms of spatial patterns, the Tarim Basin, the Sichuan Basin, and the North China Plain show high $PM_{2.5}$ pollution levels in all years. The Tarim Basin, especially the Taklamakan Desert located in the basin, always experiences sand and dust episodes, resulting in high $PM_{2.5}$ concentrations. Note that there are few ground monitoring stations in this region, so the actual situation may differ from model results. Poor meteorological conditions and the special topography affect the diffusion of pollutants in the Sichuan Basin. In the North China Plain, intensive human activities have led to substantial pollutant discharges. By contrast, $PM_{2.5}$ pollution levels are much lower in the southwestern, northeastern, and southern parts of China due to sparse human activities and temperate climatic conditions. In general, more than 99%, 98%, 71%, 68%, 64%, and 50% of the country experienced annual mean $PM_{2.5}$ concentrations exceeding the international or national acceptable air quality level (i.e., $PM_{2.5}$ = 35 μg/m^3) from 2013 to 2018, respectively.

Fig. 10 illustrates seasonal mean $PM_{2.5}$ concentrations (6-km resolution) from 2013 to 2018 in China. There is less spatial coverage in summer and winter than in spring and autumn when missing values are always observed in southern China and high-latitude areas in northern China. These areas have frequent cloudy days and surfaces covered by snow/ice, respectively, so aerosol retrieval cannot be made. There are also noticeable seasonal differences in the spatial pattern with average $PM_{2.5}$ values of 51.0 ± 19.5, 38.8 ± 14.2, 47.0 ± 20.9, and 67.2 ± 21.3 μg/m^3 in spring, summer, autumn, and winter, respectively. Winter has the most severe $PM_{2.5}$ pollution, with more than 97% of the areas failing in meeting air quality standard, especially in the BTH (~85.8 ± 26.9 μg/m^3) and YRD (~80.7 ± 12.5 μg/m^3) regions. This is because coal and fossil-fuel burning for heating dominate in northern China, leading to a large number of pollutants emitted. By contrast,

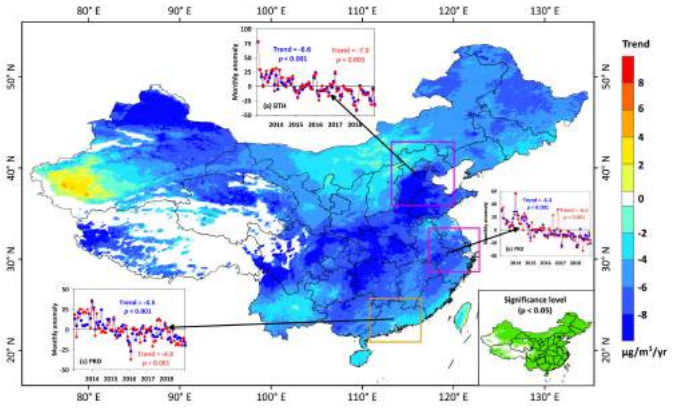

Fig. 11. Spatial distribution of trends (μg/m^3/yr^{-1}) calculated from satellite-derived deseasonalized $PM_{2.5}$ monthly anomalies from 2013 to 2018 in China. The inserted figures show time series of satellite-derived (blue color) and measured (red color) monthly $PM_{2.5}$ anomalies in three typical regions.

summer has the lowest $PM_{2.5}$ pollution level, with ~47% of mainland China below the acceptable air quality level, mainly because of the weather conditions, such as frequent precipitation. In general, spring and autumn show similar spatial patterns in $PM_{2.5}$ distributions. Note that the $PM_{2.5}$ concentrations are particularly high (>100 μg/m^3) over the Taklimakan Desert in spring and winter, mainly caused by frequent dust events and the transport of sand.

B. Temporal Variation and Trend

Fig. 11 shows the temporal $PM_{2.5}$ trends from 2013 to 2018 across mainland China. The results illustrate that $PM_{2.5}$ pollution had changed significantly in China, with an average decreasing trend of -5.6 μg/m^3/yr^{-1} ($p < 0.001$) from 2013 to 2018. In general, most of the remaining areas show significant decreasing trends in $PM_{2.5}$ concentrations ($p < 0.05$), especially in eastern and central China with large negative trends >8 μg/m^3 per year. By contrast, $PM_{2.5}$ concentrations had increasing trends >2 μg/m^3/yr^{-1} in the Tarim Basin, especially for some southwestern parts of the basin ($p < 0.05$). In addition, our satellite-derived results show that $PM_{2.5}$ pollution has significantly declined ($p < 0.001$) with average decreasing trends of 6.6, 6.3, and 4.5 μg/m^3/yr^{-1} in the BTH, YRD, and PRD regions, respectively. Meanwhile, we compared our results with $PM_{2.5}$ trends calculated from ground measurements based on surface stations in three key regions, and the same significant downward trends ($p < 0.001$) were seen from 2013 to 2018 in each region (i.e., 7.0, 6.6, and 4.8 μg/m^3/yr^{-1}), showing small differences within $\pm$0.5 μg/m^3/yr^{-1}. The differences in magnitude are caused by the different spatial coverage of satellite- and ground-based observations. Nevertheless, these results illustrate that our satellite-derived $PM_{2.5}$ temporal trends are robust.

In 2012, the Chinese government implemented a 5-year Action Plan on Air Pollution Prevention and Control (2013–2017) with the main goal of substantially reducing $PM_{2.5}$ pollution in China, especially in key regions [51]. The satellite retrievals provide an objective and independent assessment of the effect of the measures taken. Since then, $PM_{2.5}$ concentrations have decreased by 37.7%, 36.2%, 38.0%, and 26.9% over the whole of China and the BTH, PRD, and YRD regions during the Action Plan, respectively (Table III). $PM_{2.5}$ concentrations have also decreased from 72.8 $\pm$ 14.4 μg/m^3 in 2013 to 48.3 $\pm$ 6.8 μg/m^3 in 2017 in Beijing City. These results suggest that the set main pollution reduction goals by the government have been well achieved. Furthermore, the quantitative evaluation results obtained in this study are highly consistent with the official assessment results, showing small differences within 1%–4%. This shows that our VIIRS-DB-derived $PM_{2.5}$ data set captures well both the overall magnitude but also the spatiotemporal variations of $PM_{2.5}$ from which it may conclude that the emission control measures implemented in China have been effective in significantly improving the air quality [64], [65].

TABLE III

STATISTICS OF OVERALL GOALS AND COMPLETION STATUS FOR THE $PM_{2.5}$ POLLUTION CHANGE DURING THE AIR POLLUTION CONTROL PLAN

Region	Overall goal	Satellite-derived $PM_{2.5}$ results			Official results
		2013	2017	↓ by	
China	-	67.0±17.6	41.7±16.8	-37.7 %	-
EChina	-	69.9±188	45.2±10.6	-35.3 %	-
BTH	-25 %	80.3±27.2	51.2±14.2	-36.2 %	-39.6 %
YRD	-20 %	75.6±9.7	46.9±7.6	-38.0 %	-34.3 %
PRD	-15 %	62.1±7.7	45.4±5.4	-26.9 %	-27.7 %
Beijing	≈ 60	72.8±14.4	48.3±6.8	-33.6 %	= 58

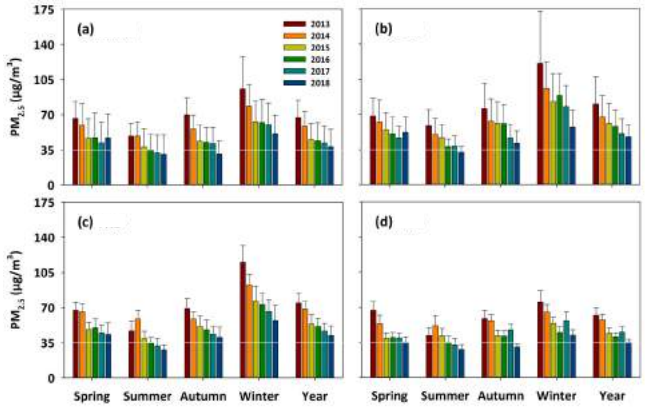

Fig. 12. Histograms of annual and seasonal mean $PM_{2.5}$ concentrations and variations from 2013 to 2018 in China and three typical regions (a) China, (b) BTH, (c) YRD, and (d) PRD.

Fig. 12 shows the histograms of annual and seasonal mean $PM_{2.5}$ concentrations and variations across China and three typical regions. $PM_{2.5}$ pollution was the most severe in 2013, when mean $PM_{2.5}$ concentrations far exceeded the acceptable air quality standard, especially in the BTH and YRD regions in winter with 2–3 times larger $PM_{2.5}$ loadings. However, by the end of 2018, $PM_{2.5}$ concentrations had gradually decreased by ~40%–45% for the whole year, and by 29%–56%, 23%–53%, 35%–51%, and 32%–49% for the four seasons in China and in three key regions. Note that the PRD region has reached a lower $PM_{2.5}$ pollution level in recent years. Overall, only the air quality in summer meets the acceptable level across China and regionally. $PM_{2.5}$ was rather high in other seasons, especially in winter. More effective measures should thus be taken in the future to control air pollution in China.

VI. Conclusion

In this study, instead of using the widely used MODIS AOD products at coarse spatial resolutions, we aimed to estimate and extend continuous observations of near-surface $PM_{2.5}$ concentrations from the newly released VIIRS Version 1 DB product at a spatial resolution of 6 km. For this purpose, the highly accurate STET model is selected following a rigorous comparison of various statistical and ML approaches to produce a spatially continuous $PM_{2.5}$ data set from 2013 to 2018 covering China, named ChinaHigh$PM_{2.5}$.

Our model works best in deriving daily $PM_{2.5}$ concentrations, with a high out-of-sample (out-of-station) CV-R^2 of 0.88 (0.87) at the national scale during 2013–2018, especially in three typical urban agglomerations. The model captures well $PM_{2.5}$ concentrations in areas with no monitoring stations. Moreover, following the implementation of the five-year (2013–2017) Action Plan on Air Pollution Prevention and Control, $PM_{2.5}$ pollution levels have systematically and significantly declined in most parts of China from 2013 to 2018 at a mean nation-wide rate of -5.6 $\mu g/m^3/yr^{-1}$ ($p < 0.001$). The satellite-based estimate of the trend from the ChinaHigh$PM_{2.5}$ is in good agreement with that from ground-based data reported by the government. The former is of high and uniform resolution and extensive spatial coverage than the latter and is thus of special value for monitoring air pollution and environmental health studies in China.

Results from this study illustrate the unique advantages of the STET model and bring new insights into satellite-based $PM_{2.5}$ estimations in China. We have made some improvements to the STET model compared to our previous study, e.g., involve and remove variables via physical mechanisms and collinearity diagnosis, and further optimized method for determining temporal and spatial information. Second, we have further analyzed the influence and sensitivity of input variables on the model performance and made detailed comparisons with traditional models and previous related $PM_{2.5}$ studies from different satellites. The results illustrate that our model is robust and has strong universality and application potential, which can be applied to different satellites. Our study provides the public with more accurate and detailed long-term spatiotemporal variations in $PM_{2.5}$ pollution across China from 2013 to 2018, including the Action Plan (2013–2017) implemented by the government, from the perspective of satellite remote sensing. This study looms the potential of extending $PM_{2.5}$ data records in China by merging the products derived from the EOS sensors (e.g., MODIS and MISR) with the VIIRS, which can be traced back to the two decades, and also extended to the next few decades after MODIS or MISR satellites retire in the future. Therefore, we will consider merging those different satellite observations to generate an integrated longer-term seamless $PM_{2.5}$ product in our future study [66].

Although our $PM_{2.5}$ estimates have good accuracy, there are still rooms for further improvement. First of all, due to complex and unclear sources of $PM_{2.5}$, more comprehensively potential natural or human variables with high spatiotemporal resolutions are strongly suggested to be involved via further literature or sensitivity tests. Then, more appropriate methods should be investigated to remove less important predictors to reduce additional noise inputs and minimize the overfitting issue caused by a large number of input variables, especially for traditional statistical regression and other artificial intelligence methods. This process can improve both model accuracy and operation efficiency. In addition, spatiotemporal information is essential and cannot be ignored in the model development; thus, more accurate determination approaches need to be explored to further improve the accuracy of $PM_{2.5}$ estimates.

Acknowledgment

The authors would like to thank Dr. Qiang Zhang, Tsinghua University, for providing MEIC pollution emission data in China. The VIIRS DB and MODIS series products are available at https://search.earthdata.nasa.gov/search. The AERONET data are available at https://aeronet.gsfc.nasa. The ChinaHigh$PM_{2.5}$ data set is available at https://weijing-rs.github.io/product.html.

References

[1] V. Ramanathan and Y. Feng, "Air pollution, greenhouse gases and climate change: Global and regional perspectives," *Atmos. Environ.*, vol. 43, no. 1, pp. 37–50, Jan. 2009.

[2] Z. Li *et al.*, "Aerosol and boundary-layer interactions and impact on air quality," *Nat. Sci. Rev.*, vol. 4, no. 6, pp. 810–833, Nov. 2017.

[3] G. Josefine, "Air pollution, climate change, and health," *Lancet Oncol.*, vol. 16, no. 6, p. e269, 2015.

[4] L. Yu, M. Zhang, L. Wang, W. Qin, and J. Li, "Aerosol radiative effects from observations and modelling over the Yangtze River Basin, China from 2001 to 2015," *Int. J. Climatol.*, vol. 39, no. 8, pp. 3476–3491, 2019.

[5] Y. Song, B. Huang, Q. He, B. Chen, J. Wei, and R. Mahmood, "Dynamic assessment of $PM_{2.5}$ exposure and health risk using remote sensing and geo-spatial big data," *Environ. Pollut.*, vol. 253, pp. 288–296, Oct. 2019.

[6] S. M. Bartell, J. Longhurst, T. Tjoa, C. Sioutas, and R. J. Delfino, "Particulate air pollution, ambulatory heart rate variability, and cardiac arrhythmia in retirement community residents with coronary artery disease," *Environ. Health Perspect.*, vol. 121, no. 10, pp. 1135–1141, Oct. 2013.

[7] R. D. Peng *et al.*, "Emergency admissions for cardiovascular and respiratory diseases and the chemical composition of fine particle air pollution," *Environ. Health Perspect.*, vol. 117, no. 6, pp. 957–963, 2009.

[8] P. Aggarwal and S. Jain, "Impact of air pollutants from surface transport sources on human health: A modeling and epidemiological approach," *Environ. Int.*, vol. 83, pp. 146–157, Oct. 2015.

[9] J. Wei *et al.*, "The ChinaHighPM_{10} dataset: Generation, validation, and spatiotemporal variations from 2015 to 2019 across China," *Environ. Int.*, vol. 146, Jan. 2021, Art. no. 106290, doi: 10.1016/j.envint.2020.106290.

[10] J. Wei *et al.*, "Estimating 1-km-resolution $PM_{2.5}$ concentrations across China using the space-time random forest approach," *Remote Sens. Environ.*, vol. 231, Sep. 2019, Art. no. 111221, doi: 10.1016/j.rse.2019.111221.

[11] R. Beelen *et al.*, "Effects of long-term exposure to air pollution on natural-cause mortality: An analysis of 22 European cohorts within the multicentre ESCAPE project," *Lancet*, vol. 383, no. 9919, pp. 785–795, 2014.

[12] J. S. Apte, J. D. Marshall, A. J. Cohen, and M. Brauer, "Addressing global mortality from ambient $PM_{2.5}$," *Environ. Sci. Technol.*, vol. 49, no. 13, pp. 8057–8066, Jul. 2015.

[13] A. J. Cohen *et al.*, "Estimates and 25-year trends of the global burden of disease attributable to ambient air pollution: An analysis of data from the global burden of diseases study 2015," *Lancet*, vol. 389, no. 10082, pp. 1907–1918, May 2017.

[14] J. Lelieveld, J. S. Evans, M. Fnais, D. Giannadaki, and A. Pozzer, "The contribution of outdoor air pollution sources to premature mortality on a global scale," *Nature*, vol. 525, no. 7569, pp. 367–371, Sep. 2015.

[15] J. Liao *et al.*, "Exposure to ambient fine particulate matter during pregnancy and gestational weight gain," *Environ. Int.*, vol. 119, pp. 407–412, Oct. 2018.

[16] J. Zhu, R. W. Lee, C. Twum, and Y. Wei, "Exposure to ambient $PM_{2.5}$ during pregnancy and preterm birth in metropolitan areas of the State of Georgia," *Environ. Sci. Pollut. Res.*, vol. 26, no. 3, pp. 2492–2500, Jan. 2019.

[17] D. Younan *et al.*, "Particulate matter and episodic memory decline mediated by early neuroanatomic biomarkers of Alzheimer's disease," *Brain*, vol. 143, no. 1, pp. 289–302, 2019.

[18] K. He, H. Huo, and Q. Zhang, "Urban air pollution in China: Current status, characteristics, and progress," *Annu. Rev. Energy Environ.*, vol. 27, no. 1, pp. 397–431, Nov. 2002.

[19] L. Sun *et al.*, "Impact of land-use and land-cover change on urban air quality in representative cities of China," *J. Atmos. Sol.-Terr. Phys.*, vol. 142, pp. 43–54, May 2016.

[20] Z. Ma, X. Hu, L. Huang, J. Bi, and Y. Liu, "Estimating ground-level $PM_{2.5}$ in China using satellite remote sensing," *Environ. Sci. Technol.*, vol. 48, no. 13, pp. 7436–7444, Jul. 2014.

[21] X. Fang, B. Zou, X. Liu, T. Sternberg, and L. Zhai, "Satellite-based ground $PM_{2.5}$ estimation using timely structure adaptive modeling," *Remote Sens. Environ.*, vol. 186, pp. 152–163, Dec. 2016.

[22] T. Xue *et al.*, "Spatiotemporal continuous estimates of $PM_{2.5}$ concentrations in China, 2000–2016: A machine learning method with inputs from satellites, chemical transport model, and ground observations," *Environ. Int.*, vol. 123, pp. 345–357, Feb. 2019.

[23] Q. He and B. Huang, "Satellite-based mapping of daily high-resolution ground $PM_{2.5}$ in China via space-time regression modeling," *Remote Sens. Environ.*, vol. 206, pp. 72–83, Mar. 2018.

[24] J. M. Jackson *et al.*, "Suomi-NPP VIIRS aerosol algorithms and data products," *J. Geophys. Res., Atmos.*, vol. 118, no. 22, pp. 12673–12689, 2013.

[25] J. Wu, F. Yao, W. Li, and M. Si, "VIIRS-based remote sensing estimation of ground-level $PM_{2.5}$ concentrations in Beijing–Tianjin–Hebei: A spatiotemporal statistical model," *Remote Sens. Environ.*, vol. 184, pp. 316–328, Oct. 2016.

[26] J. Pang *et al.*, "Assimilating AOD retrievals from GOCI and VIIRS to forecast surface $PM_{2.5}$ episodes over eastern China," *Atmos. Environ.*, vol. 179, pp. 288–304, Apr. 2018.

[27] F. Yao, M. Si, W. Li, and J. Wu, "A multidimensional comparison between MODIS and VIIRS AOD in estimating ground-level $PM_{2.5}$ concentrations over a heavily polluted region in China," *Sci. Total Environ.*, vol. 618, pp. 819–828, Mar. 2018.

[28] F. Yao, J. Wu, W. Li, and J. Peng, "A spatially structured adaptive two-stage model for retrieving ground-level $PM_{2.5}$ concentrations from VIIRS AOD in China," *ISPRS J. Photogramm. Remote Sens.*, vol. 151, pp. 263–276, May 2019.

[29] J. Wei, L. Sun, B. Huang, M. Bilal, Z. Zhang, and L. Wang, "Verification, improvement and application of aerosol optical depths in China Part 1: Inter-comparison of NPP-VIIRS and Aqua-MODIS," *Atmos. Environ.*, vol. 175, pp. 221–233, Feb. 2018.

[30] J. Wei, Z. Li, L. Sun, Y. Yang, C. Zhao, and Z. Cai, "Enhanced aerosol estimations from suomi-NPP VIIRS images over heterogeneous surfaces," *IEEE Trans. Geosci. Remote Sens.*, vol. 57, no. 12, pp. 9534–9543, Dec. 2019.

[31] N. C. Hsu *et al.*, "Enhanced deep blue aerosol retrieval algorithm: The second generation," *J. Geophys. Res., Atmos.*, vol. 118, no. 16, pp. 9296–9315, Aug. 2013.

[32] N. C. Hsu, J. Lee, A. M. Sayer, W. Kim, C. Bettenhausen, and S.-C. Tsay, "VIIRS Deep blue aerosol products over land: Extending the EOS long-term aerosol data records," *J. Geophys. Res., Atmos.*, vol. 124, no. 7, pp. 4026–4053, 2019.

[33] J. Wei, Z. Li, Y. Peng, and L. Sun, "MODIS collection 6.1 aerosol optical depth products over land and ocean: Validation and comparison," *Atmos. Environ.*, vol. 201, pp. 428–440, Mar. 2019.

[34] J. Wei *et al.*, "Improved 1 km resolution $PM_{2.5}$ estimates across China using enhanced space–time extremely randomized trees," *Atmos. Chem. Phys.*, vol. 20, no. 6, pp. 3273–3289, 2020.

[35] A. M. Sayer, N. C. Hsu, J. Lee, C. Bettenhausen, W. V. Kim, and A. Smirnov, "Satellite ocean aerosol retrieval (SOAR) algorithm extension to S-NPP VIIRS as part of the 'deep blue' aerosol project," *J. Geophys. Res., Atmos.*, vol. 123, no. 1, pp. 380–400, 2018.

[36] T.-C. Tsai, Y.-J. Jeng, D. A. Chu, J.-P. Chen, and S.-C. Chang, "Analysis of the relationship between MODIS aerosol optical depth and particulate matter from 2006 to 2008," *Atmos. Environ.*, vol. 45, no. 27, pp. 4777–4788, Sep. 2011.

[37] T. Su, J. Li, C. Li, A. K.-H. Lau, D. Yang, and C. Shen, "An intercomparison of AOD-converted $PM_{2.5}$ concentrations using different approaches for estimating aerosol vertical distribution," *Atmos. Environ.*, vol. 166, pp. 531–542, Oct. 2017.

[38] T. Su, Z. Li, and R. Kahn, "Relationships between the planetary boundary layer height and surface pollutants derived from lidar observations over China: Regional pattern and influencing factors," *Atmos. Chem. Phys.*, vol. 18, no. 21, pp. 15921–15935, Nov. 2018.

[39] Y. Zhang and Z. Li, "Remote sensing of atmospheric fine particulate matter ($PM_{2.5}$) mass concentration near the ground from satellite observation," *Remote Sens. Environ.*, vol. 160, pp. 252–262, Apr. 2015.

[40] I. N. Tang and H. R. Munkelwitz, "Water activities, densities, and refractive indices of aqueous sulfates and sodium nitrate droplets of atmospheric importance," *J. Geophys. Res., Atmos.*, vol. 99, no. D9, pp. 18801–18808, 1994.

[41] X. Jin *et al.*, "Significant contribution of organics to aerosol liquid water content in winter in Beijing, China," *Atmos. Chem. Phys.*, vol. 20, no. 2, pp. 901–914, Jan. 2020.

[42] Y. Sun *et al.*, "Investigation of the sources and evolution processes of severe haze pollution in Beijing in January 2013," *J. Geophys. Res., Atmos.*, vol. 119, no. 7, pp. 4380–4398, 2014.

[43] G. J. Zheng *et al.*, "Exploring the severe winter haze in Beijing: The impact of synoptic weather, regional transport and heterogeneous reactions," *Atmos. Chem. Phys.*, vol. 15, no. 6, pp. 2969–2983, Mar. 2015.

[44] Z. Li *et al.*, "Aerosol and monsoon climate interactions over Asia," *Rev. Geophys.*, vol. 54, no. 4, pp. 866–929, Dec. 2016.

[45] X. Wang, R. E. Dickinson, L. Su, C. Zhou, and K. Wang, "$PM_{2.5}$ pollution in China and how it has been exacerbated by terrain and meteorological conditions," *Bull. Amer. Meteorol. Soc.*, vol. 99, no. 1, pp. 105–119, Jan. 2018.

[46] Q. Zhang *et al.*, "Asian emissions in 2006 for the NASA INTEX-B mission," *Atmos. Chem. Phys.*, vol. 9, no. 14, pp. 5131–5153, Jul. 2009.

[47] M. Li *et al.*, "MIX: A Mosaic Asian anthropogenic emission inventory under the international collaboration framework of the MICS-Asia and HTAP," *Atmos. Chem. Phys.*, vol. 17, no. 2, pp. 935–963, Jan. 2017.

[48] J. H. Friedman, "Greedy function approximation: A gradient boosting machine," *Ann. Statist.*, vol. 29, no. 5, pp. 1189–1232, Oct. 2001.

[49] L. Breiman, "Random forests," *Mach. Learn.*, vol. 45, no. 1, pp. 5–32, 2001.

[50] P. Geurts, D. Ernst, and L. Wehenkel, "Extremely randomized trees," *Mach. Learn.*, vol. 63, no. 1, pp. 3–42, Apr. 2006.

[51] T. Behrens, K. Schmidt, R. A. Viscarra Rossel, P. Gries, T. Scholten, and R. A. Macmillan, "Spatial modelling with Euclidean distance fields and machine learning," *Eur. J. Soil Sci.*, vol. 69, no. 5, pp. 757–770, Sep. 2018.

[52] R. Jiang, W. Tang, X. Wu, and W. Fu, "A random forest approach to the detection of epistatic interactions in case-control studies," *BMC Bioinf.*, vol. 10, no. S1, p. 135, Jan. 2009.

[53] J. D. Rodriguez, A. Perez, and J. A. Lozano, "Sensitivity analysis of k-fold cross validation in prediction error estimation," *IEEE Trans. Pattern Anal. Mach. Intell.*, vol. 32, no. 3, pp. 569–575, Mar. 2010.

[54] T. Li, H. Shen, Q. Yuan, X. Zhang, and L. Zhang, "Estimating ground-level $PM_{2.5}$ by fusing satellite and station observations: A geo-intelligent deep learning approach," *Geophys. Res. Lett.*, vol. 44, no. 23, pp. 11985–11993, 2017.

[55] J. Wei, Y. Peng, R. Mahmood, L. Sun, and J. Guo, "Intercomparison in spatial distributions and temporal trends derived from multi-source satellite aerosol products," *Atmos. Chem. Phys.*, vol. 19, no. 10, pp. 7183–7207, May 2019.

[56] Z. Ma, R. Liu, Y. Liu, and J. Bi, "Effects of air pollution control policies on $PM_{2.5}$ pollution improvement in China from 2005 to 2017: A satellite-based perspective," *Atmos. Chem. Phys.*, vol. 19, no. 10, pp. 6861–6877, 2019.

[57] W. You, Z. Zang, L. Zhang, Y. Li, and W. Wang, "Estimating national-scale ground-level $PM_{2.5}$ concentration in China using geographically weighted regression based on MODIS and MISR AOD," *Environ. Sci. Pollut. Res.*, vol. 23, pp. 8327–8338, Jan. 2016.

[58] W. Yu, Y. Liu, Z. Ma, and J. Bi, "Improving satellite-based $PM_{2.5}$ estimates in China using Gaussian processes modeling in a Bayesian hierarchical setting," *Sci. Rep.*, vol. 7, no. 1, p. 7048, Dec. 2017.

[59] T. Li, H. Shen, C. Zeng, Q. Yuan, and L. Zhang, "Point-surface fusion of station measurements and satellite observations for mapping $PM_{2.5}$ distribution in China: Methods and assessment," *Atmos. Environ.*, vol. 152, pp. 477–489, Mar. 2017.

[60] W. You, Z. Zang, L. Zhang, Y. Li, X. Pan, and W. Wang, "National-scale estimates of ground-level $PM_{2.5}$ concentration in China using geographically weighted regression based on 3 km resolution MODIS AOD," *Remote Sens.*, vol. 8, no. 3, p. 184, Feb. 2016.

[61] Z.-Y. Chen *et al.*, "Extreme gradient boosting model to estimate $PM_{2.5}$ concentrations with missing-filled satellite data in China," *Atmos. Environ.*, vol. 202, pp. 180–189, Apr. 2019.

[62] J. Wei *et al.*, "An improved high-spatial-resolution aerosol retrieval algorithm for MODIS images over land," *J. Geophys. Res., Atmos.*, vol. 123, no. 21, pp. 12291–12307, 2018.

[63] J. Wei *et al.*, "MODIS Collection 6.1 3 km resolution aerosol optical depth product: Global evaluation and uncertainty analysis," *Atmos. Environ.*, vol. 240, Nov. 2020, Art. no. 117768.

[64] Q. Zhang *et al.*, "Drivers of improved $PM_{2.5}$ air quality in China from 2013 to 2017," *Proc. Nat. Acad. Sci. USA*, vol. 116, no. 49, pp. 24463–24469, 2019.

[65] D. Fang *et al.*, "Clean air for some: Unintended spillover effects of regional air pollution policies," *Sci. Adv.*, vol. 5, no. 4, Apr. 2019, Art. no. eaav4707.

[66] J. Wei *et al.*, "Reconstructing 1-km-resolution high-quality $PM_{2.5}$ data records from 2000 to 2018 in China: Spatiotemporal variations and policy implications," *Remote Sens. Environ.*, vol. 252, Jan. 2021, Art. no. 112136, doi: 10.1016/j.rse.2020.112136.

Jing Wei (Graduate Student Member, IEEE) received the B.Sc. and M.Sc. degrees from the Shandong University of Science of Technology, Qingdao, China, in 2014 and 2017, respectively, and the Ph.D. degree from Beijing Normal University, Beijing, China, in 2020.

He conducted the joint doctoral training at the University of Maryland, College Park, MD, USA, since 2019, where he is a Post-Doctoral Fellow. He was a Research Assistant with The Chinese University of Hong Kong, Hong Kong, China, and Tsinghua University, Beijing. He has authored more than 80 articles. His research interests include satellite cloud, aerosol, fine particulate matter, and trace gas remote sensing.

Dr. Wei is a Student Member of the American Meteorological Society (AMS) and the American Geophysical Union (AGU). He is also a Guest Editor of *Remote Sensing* and a Topic Editor of *Big Earth Data*.

Zhanqing Li received the B.Sc. and M.Sc. degrees from the Nanjing University of Information Science and Technology, Nanjing, China, in 1983 and 1986, respectively, and the Ph.D. degree from McGill University, Montreal, QC, Canada, in 1991.

He is a Professor with the University of Maryland, College Park, MD, USA. He has authored over 340 articles. His research interests include remote sensing, atmospheric physics, climate and environment focusing on aerosol, cloud, radiation budget, and precipitation.

Dr. Li is a Fellow of the American Meteorological Society (AMS), the American Geophysical Union (AGU), and the American Association for the Advancement of Science (AAAS). He received numerous awards in the USA, Canada, and Germany. He is also an Editor of *Atmospheric Chemistry and Physics*.

Lin Sun received the M.Sc. degree in meteorology from the Nanjing University of Information Science and Technology, Nanjing, China, in 2003, and the Ph.D. degree in cartography and geographic information system from the Aerospace Information Research Institute, Chinese Academy of Science, Beijing, China, in 2006.

He is a Professor with the College of Geodesy and Geomatics, Shandong University of Science and Technology, Qingdao, China. He has authored over 100 articles. His research interests include cloud detection and aerosol retrieval from satellite data.

Wenhao Xue received the B.Eng. from the Beijing University of Civil Engineering and Architecture, Beijing, China, in 2015. He is pursuing the Ph.D. degree with Beijing Normal University, Beijing.

His research interests include estimation of fine particulate matter and aerosol radiation effect.

Mr. Xue is a Student Member of the European Geosciences Union (EGU).

Zongwei Ma received the B.Sc., M.Sc., and Ph.D. degrees from Nanjing University, Nanjing, China, in 2004, 2006, and 2015, respectively. He conducted the joint doctoral training at Emory University, Atlanta, GA, USA, from 2012 to 2014.

He is an Associate Professor with Nanjing University. He has authored more than 60 peer-reviewed articles. His research interests include exposure and health risks of air pollution, environmental risk assessment, and risk management.

Dr. Ma is a member of the American Geophysical Union (AGU). He received two sci-tech awards from the Ministry of Education of China and the Society of Management Science of China.

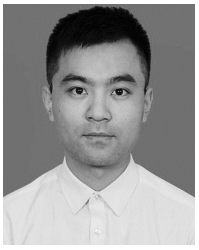

Lei Liu received the Ph.D. degree in geography from the International Institute for Earth System Science, Nanjing University, Nanjing, China, in 2019.

He is a Professor with the College of Earth and Environmental Sciences, Lanzhou University, Lanzhou, China. He has authored over 50 articles. His research interest includes atmospheric remote sensing.

Tianyi Fan received the B.Sc. and M.Sc. degrees from Sun Yat-sen University, Guangzhou, China, in 2003 and 2005, respectively, and the Ph.D. degree from the University of Colorado at Boulder, Boulder, CO, USA, in 2012.

She is a Junior Research Scientist with Beijing Normal University, Beijing, China. She has authored more than 20 articles. Her research interests include aerosol, cloud, and climate models.

Dr. Fan is a member of the American Geophysical Union (AGU).

Maureen Cribb, photograph and biography not available at the time of publication.